5-2014

# Intercomparison of field measurements of nitrous acid (HONO) during the SHARP campaign

J R. Pinto
*U.S. Environmental Protection Agency*

Jack E. Dibb
*University of New Hampshire*, jack.dibb@unh.edu

B H. Lee
*University of Washington - Seattle Campus*

B Rappengluck
*University of Houston - Main*

E C. Wood
*University of Massachusetts - Amherst*

***See next page for additional authors***



## Recommended Citation

Pinto, J. P., et al. (2014), Intercomparison of field measurements of nitrous acid (HONO) during the SHARP campaign, J. Geophys. Res. Atmos., 119, 5583–5601, doi:10.1002/2013JD020287.

AGU PUBLICATIONS

JGR

Journal of Geophysical Research: Atmospheres

RESEARCH ARTICLE
10.1002/2013JD020287

Special Section:
Study of Houston Atmospheric Radical Precursors (SHARP)

# Intercomparison of field measurements of nitrous acid (HONO) during the SHARP campaign

**J. P. Pinto[1], J. Dibb[2], B. H. Lee[3], B. Rappenglück[4], E. C. Wood[5,6], M. Levy[7], R.-Y. Zhang[7], B. Lefer[4], X.-R. Ren[8,9], J. Stutz[10], C. Tsai[10], L. Ackermann[4], J. Golovko[4], S. C. Herndon[6], M. Oakes[11], Q.-Y. Meng[12], J. W. Munger[13], M. Zahniser[6], and J. Zheng[7,14]**

[1]National Center for Environmental Assessment, U.S. Environmental Protection Agency, Durham, North Carolina, USA, [2]Institute for the Study of Earth, Oceans and Space, University of New Hampshire, Durham, New Hampshire, USA, [3]Department of Atmospheric Science, University of Washington, Seattle, Washington, USA, [4]Department of Earth and Atmospheric Sciences, University of Houston, Houston, Texas, USA, [5]Department of Environmental Health Sciences, University of Massachusetts Amherst, Amherst, Massachusetts, USA, [6]Aerodyne Research Inc., Billerica, Massachusetts, USA, [7]Department of Atmospheric Science, Texas A&M University, College Station, Texas, USA, [8]Rosentiel School of Marine and Atmospheric Science, University of Miami, Coral Gables, Florida, USA, [9]Now at NOAA/Air Resources Laboratory, National Oceanic and Atmospheric Administration, College Park, Maryland, USA, [10]Department of Atmospheric and Oceanic Sciences, University of California, Los Angeles, California, USA, [11]Oak Ridge Institute for Science Education, Oak Ridge, Tennessee, USA, [12]Department of Environmental and Occupational Health, University of Medicine and Dentistry of New Jersey, Piscataway, New Jersey, USA, [13]School of Engineering and Applied Science, Harvard University, Cambridge, Massachusetts, USA, [14]Now at Nanjing University of Information Science and Technology, Nanjing, China

**Key Points:**
- HONO was measured by six techniques during SHARP under polluted urban conditions
- Methods with collocated inlets tracked each other most closely
- Differences between techniques not likely explained by chemical interference alone

**Supporting Information:**
- Readme
- Tables S1–S3 and Figures S1–S13
- Text S1

**Correspondence to:**
J. P. Pinto,
pinto.joseph@epa.gov

**Citation:**
Pinto, J. P., et al. (2014), Intercomparison of field measurements of nitrous acid (HONO) during the SHARP campaign, *J. Geophys. Res. Atmos.*, *119*, 5583–5601, doi:10.1002/2013JD020287.

Received 30 MAY 2013
Accepted 5 APR 2014
Accepted article online 9 APR 2014
Published online 5 MAY 2014

**Abstract** Because of the importance of HONO as a radical reservoir, consistent and accurate measurements of its concentration are needed. As part of SHARP (Study of Houston Atmospheric Radical Precursors), time series of HONO were obtained by six different measurement techniques on the roof of the Moody Tower at the University of Houston. Techniques used were long path differential optical absorption spectroscopy (DOAS), stripping coil-visible absorption photometry (SC-AP), long path absorption photometry (LOPAP®), mist chamber/ion chromatography (MC-IC), quantum cascade-tunable infrared laser differential absorption spectroscopy (QC-TILDAS), and ion drift-chemical ionization mass spectrometry (ID-CIMS). Various combinations of techniques were in operation from 15 April through 31 May 2009. All instruments recorded a similar diurnal pattern of HONO concentrations with higher median and mean values during the night than during the day. Highest values were observed in the final 2 weeks of the campaign. Inlets for the MC-IC, SC-AP, and QC-TILDAS were collocated and agreed most closely with each other based on several measures. Largest differences between pairs of measurements were evident during the day for concentrations ~100 parts per trillion (ppt). Above ~200 ppt, concentrations from the SC-AP, MC-IC, and QC-TILDAS converged to within about 20%, with slightly larger discrepancies when DOAS was considered. During the first 2 weeks, HONO measured by ID-CIMS agreed with these techniques, but ID-CIMS reported higher values during the afternoon and evening of the final 4 weeks, possibly from interference from unknown sources. A number of factors, including building related sources, likely affected measured concentrations.

## 1. Introduction

The importance of nitrous acid (HONO) as a precursor of OH radicals that initiate photochemical processes in the atmosphere has long been recognized. Nitrous acid can be emitted from traffic, in particular diesel vehicles [*Rappenglück et al.*, 2013]. Nitrous acid emitted or formed from motor vehicle exhaust at night has long been suspected to be a significant source of radicals shortly after sunrise, which in turn could "jump start" photochemical smog formation [e.g., *Mao et al.*, 2010; *Olaguer et al.*, 2009; *Elshorbany et al.*, 2009; *Acker et al.*, 2006; *Kleffmann et al.*, 2005; *Aumont et al.*, 2003; *Alicke et al.*, 2002]. However, combustion is not the only source of HONO to the atmosphere. Rather, it can also be produced by heterogeneous reactions occurring on various types of surfaces. Such multiphase reactions might take place on soil or man-made surfaces, such as buildings and roadways, or on airborne particles. Several studies have shown that multiphase reactions on various surfaces yield significant amounts of HONO throughout the entire day [see, e.g., *Czader et al.*, 2012; *Wong et al.*, 2012].

HONO sources driven by multiphase processes coupled with its potential importance for atmospheric photochemistry spurred interest in studying heterogeneous reactions. On the other hand, this characteristic suggests that measurements of HONO could be subject to production on instrument inlets [see, e.g., *Zhou et al.,* 2002], and/or because HONO is highly reactive on surfaces, its measurement could also be subject to negative artifacts unless measures, such as the use of Teflon lines, are taken to minimize potential artifacts.

Given the widespread interest in HONO and the necessity for its accurate measurements, a number of field campaigns have conducted intercomparisons. In an intercomparison between a folded-path differential optical absorption spectrometer (DOAS) and a long path absorption photometer (LOPAP®) (in Milan, Italy), *Kleffmann et al.* [2006] found quite good agreement (regression slope = 0.987 ± 0.015, intercept = −13 ± 17 ppt, $R^2 = 0.87$). This good agreement is largely due to minimizing sampling artifacts and measuring and correcting potential interfering compounds. It is during daytime that HONO concentrations are at their lowest in a 24 h cycle and when the effects of potential interfering species are most apparent. The FIONA (Formal Intercomparisons of Observations of Nitrous Acid) Campaign comparing 18 instruments in 10 experiments for measuring HONO was carried out at the European Photoreactor simulation chambers in May 2010 [*Ródenas et al.*, 2013]. Some interference by nitrites was found [*Ródenas et al.*, 2013]; however, nitrite levels were orders of magnitude above atmospheric concentrations. In the FIONA campaign, the HONO concentration range extended to very high values, e.g., 15 ppb in the early stages of the comparisons. At these high concentrations of HONO, concentrations of species potentially causing interference are dwarfed by concentrations of HONO. As a result, regression parameters, which can in many cases be strongly influenced by values at the upper end of the measured range, would tend to indicate better agreement than might be expected if intercomparisons were carried out only at much lower ambient levels. However, most experiments were conducted in the 0.5–3 ppb range, representing urban and semirural conditions.

During the TRAMP (Texas Radical and Aerosol Measurement) project, HONO measurements by DOAS and mist chamber-ion chromatography were compared [*Stutz et al.*, 2010] on the campus of the University of Houston (UH). UH is located approximately 4 km SE of downtown Houston, TX, and about 10 km to the west of the Houston Ship Channel. Measurements of HONO concentrations by the mist chamber, located on the roof of Moody Tower were consistently higher than those measured by the DOAS in low-path mode. *Stutz et al.* [2010] noted that "…measurement of HONO is problematic, with most *in-situ* techniques reporting higher values than simultaneous optical measurements by long path DOAS, especially during daytime. The discrepancy has been attributed to positive interference in the *in-situ* techniques, negative interference in DOAS retrievals, the difficulty of comparing the different air masses sampled by the methods, or combinations of these (factors)."

These observations are largely responsible for the initiation of HINT (HONO intercomparison)—a component of the SHARP (Study of Houston Atmospheric Radical Precursors) campaign that was carried out on the roof of Moody Tower during spring 2009. For the HINT study, six HONO instruments were operated for different lengths of time from 15 April to 30 May 2009 on top of Moody Tower (~65 m). All HONO instruments were operational from May 16 to 30. This period will be referred to as the common measurement period (CMP). The sampling campaign can be conveniently separated into three consecutive, 2 week periods based on atmospheric conditions and when instruments began collecting data. HINT was originally planned to be a formal, blind, intercomparison and during the first week or so no data were shared. However, personal matters that arose during the first week of the campaign prevented the referee from participating, so the investigators agreed to conduct the intercomparison on an open basis throughout the remainder of the SHARP campaign. Although not done in a systematic way, a common HONO standard and data were shared among participants and results were discussed with the intention of identifying and possibly remedying potential problems in individual instruments. The intercomparison carried out at the University of Houston differed somewhat from those described by *Kleffmann et al.* [2006] and by *Ródenas et al.* [2013] in the number of different instruments included and that it was conducted entirely under ambient urban conditions, i.e., at atmospherically relevant concentrations characterized by exposure to real world atmospheric chemical matrices for 6 weeks. It should also be noted that in this intercomparison, specific versions of instruments under conditions specific to Houston are compared and results obtained here do not necessarily apply to other locations.

**Table 1.** Instruments Compared During the SHARP Field Study

| Instrument | Group | Sampling Period | Sampling Frequency | Detection Limit | Stated Uncertainty | Reference |
|---|---|---|---|---|---|---|
| Long path-differential optical absorption spectrometer | UCLA | 4/15–5/30 | Variable (3–22 min) | Variable (16–200 ppt). 32 ppt estimated during SHARP | 10% | *Platt et al.* [1980] and *Platt and Stutz* [2008] |
| Mist chamber/ion chromatography | U New Hampshire | 4/16–5/30 | 5 min | 5 ppt | 10% | *Scheuer et al.* [2003] and *Dibb et al.* [1994, 2004] |
| Stripping coil-(visible) absorption photometer | U Miami | 4/19–5/30 | 2 min | 5 ppt | 15% | *Ren et al.* [2010] |
| Ion drift-chemical ionization mass spectrometer | Texas A&M | 4/20–5/30 | 1 s | 10–20 ppt | 25% | *Zhang et al.* [1996] and *Zheng et al.* [2008] |
| Tunable infrared laser differential absorption spectrometer-continuous wave quantum cascade laser | Harvard U/Aerodyne | 5/2–5/30 | 30 min | 60 ppt | 15% | *Lee et al.* [2011, 2012] |
| Long path absorption photometer | U Houston | 5/16–5/30 | 1 min | 5 ppt | 10% | *Kleffmann et al.* [2006] |

## 2. Methods

### 2.1. Sampling Instrumentation

The six instruments, the groups operating them, and selected specifications are shown in Table 1. The long path-differential optical absorption spectrometer (LP-DOAS) is described in *Platt et al.* [1980] and *Platt and Stutz* [2008], the mist chamber with ion chromatography (IC) detection is described in *Scheuer et al.* [2003] and *Dibb et al.* [1994, 2004], the stripping coil-visible light spectrometer (VIS) absorption photometer (SC-AP) is described in *Ren et al.* [2010], the ion drift-chemical ionization mass spectrometer (ID-CIMS) is described in *Zhang et al.* [1996] and *Zheng et al.* [2008], the Harvard/Aerodyne continuous wave-tunable infrared laser differential absorption spectrometer (TILDAS) is described in *Lee et al.* [2011], and the long path absorption photometer (LOPAP) is described in *Kleffmann et al.* [2006, and references therein]. Brief descriptions of the instruments included here and several other instruments for measuring HONO can also be found in the review by *Zhou* [2013].

The arrangement of the sampling instruments on top of Moody Tower is shown schematically in Figure S1 in the supporting information. Briefly, the inlets of the mist chamber (MC)-IC, quantum cascade (QC)-TILDAS, and SC-AP were collocated at the top of a 6 m tall scaffolding tower. Inlets for the ID-CIMS and LOPAP were placed at heights of ~2.5 m on separate masts several meters away from the scaffolding tower sampling on the east side of the Moody Tower. The telescope for the DOAS was located on the opposite side of the roof of Moody Tower facing northwest towards downtown Houston.

A gas phase HONO source was developed to quantitatively produce HONO with high purity and high stability and was used to calibrate and test all the in situ instruments. This source is based on the reaction between gaseous hydrogen chloride (HCl) and solid sodium nitrite ($NaNO_2$), and its details are described elsewhere [*Febo et al.*, 1995; *Ren et al.*, 2010]. The HONO source was able to produce HONO levels varying over 3 orders of magnitude, from a few tens of parts per trillion by volume (pptv) to a few tens of ppbv. The HONO concentration in the source was quantified with an NO-$NO_x$ analyzer (TEI, Model 42i-TL, Thermo Fisher), which was calibrated with a cylindered NO calibration mixture. The overall uncertainty of the gas phase HONO source is estimated to be about ±4% arising from uncertainties in the NO standard (±2%, Matheson Tri-Gas), mass flow controllers (~±3%), and the measurements by the NO-$NO_x$ analyzer (~±2%). The measurements of the HONO source by each in situ instrument are roughly within the combined uncertainty of the HONO source and each individual instrument (cf. Table 1). Figure S2 in the supporting information shows results of challenges of the in situ instruments by the HONO source. Greater detail can be found in the separate file, "SI HONO calibration." Available regression parameters for instruments comparing the calibration HONO source include: for MC-IC,

slope = 1.06, intercept = 23.5, $R^2 = 0.89$; for SC-AP, slope = 0.99, intercept = 0.002, $R^2 = 0.99$. Note the HONO source was not used as a primary calibration for any of the instruments as each instrument has its own primary calibration method as described below.

#### 2.1.1. DOAS

The University of California, Los Angeles (UCLA), DOAS instrument consists of a 1.5 m double Newtonian telescope, which is used to send a parallel beam of light from a Xe arc lamp onto an array of quartz corner cube retroreflectors. The light returning from the retroreflectors is received by the same telescope and, through a fiber mode mixer, fed into a 500 mm Czerny-Turner Spectrometer (ACTON Spectra-Pro 500) with a photodiode array detector (Hoffmann Messtechnik). In Houston the LP-DOAS measured the atmospheric absorptions of $O_3$, HCHO, $NO_2$, $NO_3$, HONO, and $SO_2$ between the telescope and three retroreflector arrays in downtown Houston at a distance of 4–5 km. Measurements alternated between the retroreflectors at three different heights. Because of the multiple light paths, DOAS measurements on particular light paths were made consecutively. Here we concentrate on the lowest path which averaged over the 20–70 m height interval, which will be referred to simply as DOAS. The measurement interval for the DOAS varied from 3 to 22 min depending on visibility. The systematic error in HONO retrievals due to uncertainty in HONO cross sections was 5%. The systematic error of the DOAS spectrometer was $<3\%$ [*Platt and Stutz*, 2008]. A campaign average detection limit of 32 ppt was derived for conditions during the SHARP campaign. As the detection limit of DOAS observations depend on atmospheric conditions, such as visibility, and turbulence, lower detection limit, down to ~10 ppt, are possible. A typical example of a long path DOAS HONO measurement with a mixing ratio of $0.139 \pm 0.013$ ppb, for a relative error of ~10%, was obtained by *Wong et al.* [2012].

#### 2.1.2. MC-IC

Mixing ratios of $HNO_3$ and HONO were quantified at 5 min resolution with the same University of New Hampshire dual-channel, mist chamber-ion chromatography system used for the TRAMP experiment as described by *Stutz et al.* [2010]. As during TRAMP, the samplers and ICs were deployed in an enclosure half way up the walkup tower, with a 3 m long heated perfluoroalkoxy (PFA) Teflon inlet reaching to the top of the tower, adjacent to the inlets used for the QC-TILDAS and SC-AP. The only significant changes in operation compared to TRAMP were that sampling could be conducted for 4.5 days (compared to ~40 h) between maintenance interruptions (to replenish eluent, sampler fill water, and recalibrate the ICs with National Institute of Standards and Technology traceable aqueous standards) and that the HONO standard provided by University of Miami could be occasionally sampled to confirm inlet passing efficiency. These tests all showed quantitative (i.e., 100%) recovery of the gas phase HONO standard added to our 50 standard liter per minute flow of air containing ambient HONO. This method assumes that the mixing ratio of HONO in the atmosphere varies smoothly over the 30 min of each test and that ambient HONO could be estimated from measurements immediately before and after each test. Because sampling was done at such a high flow rate, pure gas phase standard could not be sampled, and it was necessary to do standard additions. As during TRAMP, the detection limit for 5 min sample integration was $<5$ ppt, and the uncertainty in reported ambient mixing ratios was ~10%.

#### 2.1.3. SC-AP

The University of Miami stripping coil-visible absorption photometer is based on aqueous scrubbing of HONO followed by nitrite derivatization to a highly light-absorbing azo dye, which is then detected with liquid waveguide long-path absorption [*Ren et al.*, 2010]. The derivatization to the azo dye is completed through the nitrite reaction with sulfanilamide (SA) and N-(1-naphthyl) ethylenediamine. A few modifications from *Ren et al.* [2010] were made for this instrument in this field deployment. First, similar to a LOPAP instrument, a tubeless HONO sampler was used to eliminate potential interferences associated with the sample inlet. Second, two coil samplers in series were used, with the upstream sampler measuring the total signal and the downstream sampler measuring the background/interfering signal. The difference between the two signals is the HONO signal. Third, the sample analysis unit and data acquisition unit were housed inside a small weatherproof shelter located on top of the scaffolding tower to minimize the distance between the sampler and the analysis unit so that the inlet could be collocated with the inlets for MC-IC and QC-TILDAS on top of the scaffolding tower. The SC-AP instrument was calibrated every 2–3 days using sodium nitrite ($NaNO_2$) standard solutions as well as a gas phase HONO source. The detection limit of SC-AP was about 3 pptv with a 2 min integration time, and the measurement uncertainty was about ±15% at the 2σ confidence level.

A small interference signal from $NO_2$ was collected in the downstream coil sampler and was subtracted from the total signal collected in the upstream sampler. Possible interference from $SO_2$, $HNO_3$, and other nitrogen species (e.g., inorganic nitrate, peroxyacetylnitrate (PAN), and other organic nitrates) was also examined, but no significant interference was found [*Ren et al.*, 2010].

#### 2.1.4. ID-CIMS

The ID-CIMS system consisted of an ion source to produce the reagent ions, a drift tube where the ion-molecule reaction took place, and a quadrupole mass spectrometer where the reagent and product ions were analyzed [*Zhang et al.*, 1996; *Zheng et al.*, 2008]. The ID-CIMS HONO inlet was made of PFA tubing, 3.7 m long and 1.4 cm OD that protruded about 1.2 m above the roof of an air-conditioned trailer on the north Moody Tower. A diaphragm pump was used to pull >20 sLpm (standard liters per minute) air into the inlet, which reduced the residence time in the inlet to below 0.13 s. Sulfur hexafluoride anion ($SF_6^-$) was utilized for HONO detection according to *Zhang et al.* [1996]. A stream of nitrogen doped with trace amount of $SF_6$ (<0.1%) was introduced into a corona discharge region, and the reagent ion $SF_6^-$ was produced [*Zhao et al.*, 2005; *Wang et al.*, 2010], $SF_6 + e^- \rightarrow SF_6^-$. $SF_6^-$ reacted with HONO to form $F^-$ HONO through fluoride transfer reaction, which was detected by the mass spectrometer according to $SF_6^- + HONO \rightarrow SF_5 + F^- \cdot HONO$. Note that unlike a typical CIMS flow tube configuration [*Molina et al.*, 1997], water clusters of the fluoride anion ($F^- \cdot (H_2O)_n$, $n = 0, 1, 2\ldots$) were below 10% of the primary reagent ion under ambient conditions, indicating that the drift tube effectively broke up weakly bonded water clusters [*Zhao and Zhang*, 2004] and applying for the first time, the $SF_6^-$-HONO ion-molecular chemistry scheme to the humid, semitropical troposphere.

The ID-CIMS was calibrated using two independent methods that agreed with each other to within 5%. First, pure $N_2$ was bubbled through a synthesized HONO solution and guided into a quartz absorption cell inside a UV/VIS photospectrometer (Perkin Elmer), where HONO and $NO_2$ (resulting from the dissociation of HONO) optical absorbance at 354 nm and 368 nm were measured. From this, the absolute concentration of the HONO concentration in the optical cell was derived. Secondly, an alternative portable HONO calibration device was used, which consisted of a homemade Teflon® $NaNO_2$ column and an $HNO_3$ permeation tube [*Zheng et al.*, 2008]. Briefly, about 200 $cm^3\ min^{-1}$ STP $N_2$ was moved into a temperature-controlled (40°C and 1 atm.) U-shaped glass tube housing a $HNO_3$ permeation tube (VICI Metronics). $HNO_3$ vapor produced in the permeation tube was carried into a $NaNO_2$ column, where HONO was produced from $HNO_3$, $HNO_3 + NaNO_2 \rightarrow HONO + NaNO_3$. Calibrations using the $HNO_3$ permeation device were conducted daily around noontime, when HONO concentrations were low. Typical sensitivity of the ID-CIMS for HONO was 200–300 counts per second/ppb, yielding a detection limit of 10–20 ppt for a 1 s integration time. A computer-controlled three-way Teflon valve (Cole Parmer) was used to direct the sample flow through either the charcoal denuder or the PFA inlet to conduct automatic background checks every 6 min. The uncertainty of ID-CIMS for HONO measurements was estimated to be about 25%, including the systematic error and the error related to calibration.

#### 2.1.5. QC-TILDAS

Mixing ratios of HONO and $NO_2$ were simultaneously quantified using a dual quantum cascade-tunable infrared laser differential absorption spectrometer (QC-TILDAS), capable of fast time response measurements. This dual QC-TILDAS instrument is described in detail by *Lee et al.* [2011]. Ambient air was continuously drawn from the top of a four-story scaffolding tower through a custom-built siloxyl-coated quartz inlet, connected by 30 feet (9.2 m) of 3/8 inch (9.5 mm) outer diameter perfluoroalkoxy (PFA) tubing to the spectrometer. The inlet removed particles larger than about 4 μm (in aerodynamic diameter) from the sample stream by inertial separation, allowing ambient sampling without the need for filters. A critical orifice installed at the inlet of the sampling line immediately reduced the pressure of the sampled air prior to entering the transit tube so that the pressure inside the 5 L sampling cell was maintained at around 40 hPa. At a mass flow rate of 10 sLpm, average residence times in the inlet, tubing, and sampling cell were 0.3, 0.2, and 1.2 s, respectively. Both the inlet and tubing were heated to 35°C and covered by opaque materials. The combination of reduced pressure and heating minimized the presence of aqueous films in the sample line. The transmission of HONO was periodically quantified by standard additions of HONO to the inlet while sampling ambient air. Standard additions of $NO_2$ were also conducted while sampling ambient air to quantify its interference but no additional HONO signal was found, even at $NO_2$ mixing ratios > 200 ppb. Details of these transmission and interference tests are described in *Lee et al.* [2011]. Quantification of HONO in the field relies on the accuracy of midinfrared line strengths for

absorption features in the 1659.5–1659.7 $cm^{-1}$ region, obtained in the laboratory by measuring the absorbance of HONO by the spectrometer while quantifying HONO by complete catalytic conversion to NO, followed by calibrated absorption spectroscopy [*Lee et al.*, 2012].

#### 2.1.6. LOPAP®

The LOPAP® (long path absorption photometry) instrument is commercially available (QUMA Elektronik & Analytik GmbH, Wuppertal, Germany). It is described in detail by *Heland et al.* [2001] and *Kleffmann et al.* [2002]. It is a wet chemical in situ instrument consisting of an external sampling unit in which ambient gaseous HONO is directly sampled in a stripping coil using a mixture of sulfanilamide in hydrochloric acid. The external sampling unit was about 2.5 m above the roof level positioned over the railing of the east side of the Moody Tower. No sampling lines are used, thus minimizing sampling artifacts on surfaces. The stripping reagent is transferred through an insulated transfer line (length: 3 m; outer diameter 5 cm; kept at 20C°) to the instrument where it is converted to an azo dye by the reaction with N-naphtylethylendiaminedihydrochloride. The absorption of the light from a white light-emitting diode is measured in long-path absorption tubes made of Teflon AF2400 using a minispectrometer. In the external sampling unit two stripping coils are used in series. In the first channel HONO as well as possible interferences are determined, while in the second channel only the interferences are quantified. The difference of these two channels yields the HONO signal.

The sampling time during SHARP was 1 min. The time delay, i.e., the time it takes to observe the first change in the signal due to an external input, was 12.2 min (standard deviation (SD) ~ 1 min). The response time, i.e., the time it takes for the signal to go from 100% to 10% of the initial value or from 0% to 90% of the final value, was 5.9 min (SD ~ 0.5 min). The time correction used to create the time stamp reported was equal to the sum of the time delay and half the response time, or 15.2 min (SD ~ 1 min), and was determined largely by the delay time.

In order to determine the zero baseline, ultrahigh purity nitrogen (ultrahigh purity (UHP) $N_2$) was applied every 8 h for 20 min directly to the inlet of the external sampling unit by a 1/32 inch PFA tubing which was partially inserted into the tip of the stripping coil. A linear (or polynomial) function that fits the zero readings was calculated and used as the zero baseline. A zero baseline check was also performed right before any calibrations of the instrument. For the calibration itself, the stripping solution was replaced by 0.01 mg $NO_2^-$ per liter stripping solution, while UHP $N_2$ was flowing into the inlet of the external sampling unit. Final calibration values were calculated using the calibration standard concentration and the measured gas and liquid flow rates. Five calibrations were performed during the time frame 16 May to 1 June 2009, which encompasses the time frame the UH LOPAP participated in the intercomparison. The detection limit during SHARP was 5 ppt ± 10%. Calibrations yielded an averaged precision of 2% and an overall uncertainty of 10% ± 23 ppt.

Two of the instruments had novel aspects. As noted above the ID-CIMS applied, for the first time, the $SF_6^-$-HONO ion-molecular chemistry scheme for HONO detection to the humid, semitropical troposphere; and the QC-TILDAS was first deployed in a long-duration field campaign. In addition to the measurements of HONO during SHARP, ancillary measurements of speciated C2-C10 hydrocarbons, other VOCs (including formaldehyde and acetaldehyde), $HO_x$ (OH, $HO_2$), peroxides ($H_2O_2$, $CH_3OOH$), $NO_x$ (NO, $NO_2$), and $NO_z$ species ($HNO_3$, PAN, and PPN), photolysis rates of chemically important species, and meteorological parameters (temperature, pressure, and relative humidity) were also made available to aid in the interpretation of results (see *Ren et al.* [2013] for a description of these measurements).

### 2.2. Data Analysis

Several types of analyses, designed to examine different concentration ranges and environmental conditions were performed comparing all possible combinations of pairs of instruments. These are presented in the order of DOAS-low path, mist chamber (MC-IC), SC-AP, ID-CIMS, and QC-TILDAS as the independent variable. The order reflects length of record of each of the instruments taken as the independent variable. Sampling times and intervals varied widely across the methods, from seconds to minutes. Since the DOAS had the longest sampling times, samples from the other techniques were averaged over the sampling period of the DOAS subject to the criterion that there was 75% coverage of the sampling interval of the DOAS. Some other technique, such as using the median or averaging all of the methods and then comparing individual

techniques to this ensemble median or mean might be appropriate if the objective was to determine best estimates of the HONO concentrations during the field study, but would provide no information on the suitability of any of the methods as a measurement technique at other times or places.

Individual data sets were merged using IGOR and referenced to DOAS time stamps. Time series of concentration data were analyzed using statistical routines in IGOR (WaveMetrics, Inc., Portland, OR), SAS (SAS, Inc., Cary, NC), and STATA (StataCorp, College Station, TX).

## 3. Results

Figures 1a to 1c show time series of HONO measurements made by the different techniques for three successive periods, 15 April (the start of the SHARP campaign) to 1 May, 5 May to 16 May, and 16 May to 30 May. The choice of periods for parsing the data set reflects the dates for which different instruments became operational and overall differences in HONO concentrations between periods. Figures 2a to 2c show the diel variation of hourly average HONO concentrations measured by the instruments for the same 2 week periods as in Figures 1a to 1c. As can be seen from Figures 1a to 1c and 2a to 2c, concentrations measured by all the instruments tended to be higher during the night than during the day, with lowest concentrations observed during afternoon. Spikes in concentrations are apparent in the time series of all techniques and occur mainly at night. Highest HONO concentrations and the largest diel variation occurred during the last 2 weeks of the sampling campaign, i.e., the common measurement period (CMP). Most of the preceding 4 weeks was characterized by much lower concentrations, as in the second week of the sampling campaign, than during the CMP.

### 3.1. Summary Statistics

Overall, the HONO data record showed a very large dynamic range of about a factor of 1000 between highest and lowest values. Summary statistics (median, mean, standard deviation, maximum, and minimum) for all instruments during their entire period of operations are shown in Table 2. The first four instruments in the table (DOAS, MC-IC, SC-AP, and ID-CIMS) had comparable periods of operation and showed good agreement; median or mean concentrations differed by ~ 20%; and all instruments reported similar high values. The large differences between median and mean values shown in Table 2 provide an indication that the means were strongly influenced by spikes of high concentrations, especially during the last 2 weeks of the campaign. Note from Figure 1 that most of the measured concentrations were less than 1 ppb.

During daytime (0900–1700) of the first 2 weeks of the campaign, reported median (mean) concentrations ranged from 46 (49 ppt) for SC-AP and 47 (53 ppt) for ID-CIMS to 80 ppt (62 ppt) for the DOAS. Median (mean) nighttime (2000–0700) concentrations are higher, 65 to 130 ppt, (121 to 149 ppt) with lowest values reported by the SC-AP and highest values reported by the DOAS. During the first 2 weeks of the campaign, Figure 2a shows that concentrations measured by ID-CIMS were most often within the range of those measured by the other instruments, but Figures 2b (for weeks 3 and 4) and 2c (for weeks 5 and 6) show that hourly mean concentrations measured by ID-CIMS were typically higher than reported by the other instruments during the afternoon and evening. This could have been related to interference from unknown sources, including an environmental chamber used to investigate soot aging from flame combustion that was located close to the inlet for the ID-CIMS. At the beginning of the second 2 week period (see Figure 2b) the QC-TILDAS initiated sampling. Also, during weeks 3 and 4, lowest median (mean) daytime concentrations were reported by the QC-TILDAS 47 (59 ppt) and highest values were reported by the ID-CIMS 118 ppt (125 ppt). Median (mean) nighttime concentrations are higher, ranging from 84 ppt (108 ppt) for the mist chamber to 120 ppt (187 ppt) for ID-CIMS.

During the third, 2 week, period the LOPAP (University of Houston) came online. During daytime, lowest median (mean) daytime concentrations were reported by the DOAS 80 ppt (80 ppt) and highest values were reported by the ID-CIMS 177 ppt (206 ppt). Median (mean) nighttime concentrations are higher, ranging from 231 ppt (324 ppt) for the LOPAP to 428 ppt (445 ppt) for ID-CIMS, and exhibited considerably more scatter. In contrast to the first 4 weeks of the campaign, the DOAS reported lowest median (mean) concentrations and nighttime concentrations for all instruments are significantly higher. Summary statistics for these three 2 week periods on an individual basis are given in Table S1 for day and night combined, in Table 2 for day alone and Table S3 for night alone.

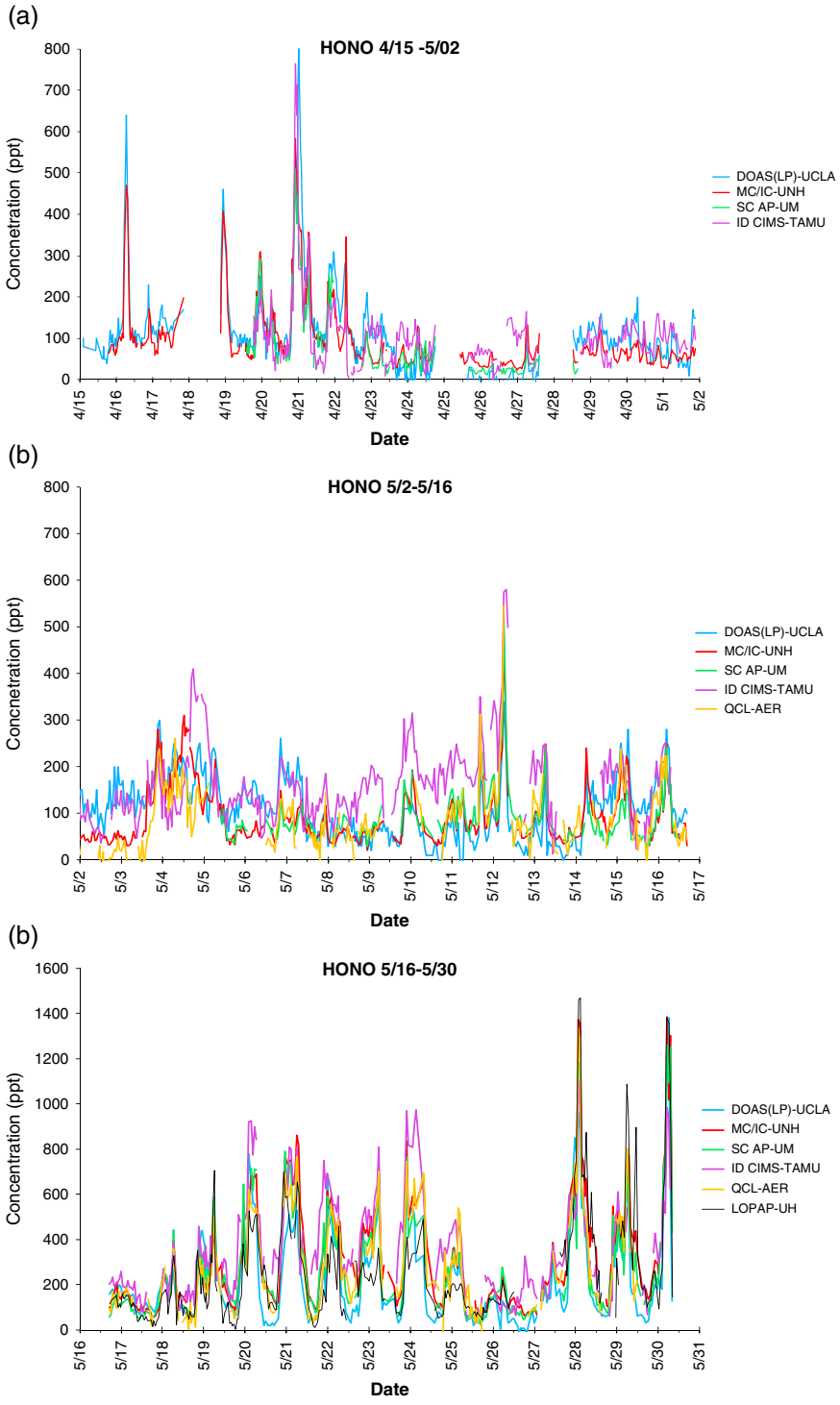


**Figure 1.** (a) Time series of HONO measurements by different techniques from 15 April to 1 May 2009. (b) Time series of HONO measurements by different techniques from 1 May to 16 May 2009. (c) Time series of HONO measurements by different techniques from 16 May to 30 May 2009.

Ordinary least squares (OLS) regression parameters (slope ± standard error, intercept ± standard error, $R^2$, and number of pairs) for the entire period of joint operation of the instruments are shown in Table 3. Independent variables are shown after the dependent variables, and the order of the independent variables reflects the length of time the instrument was in operation. In addition, since there are errors in the independent variable,

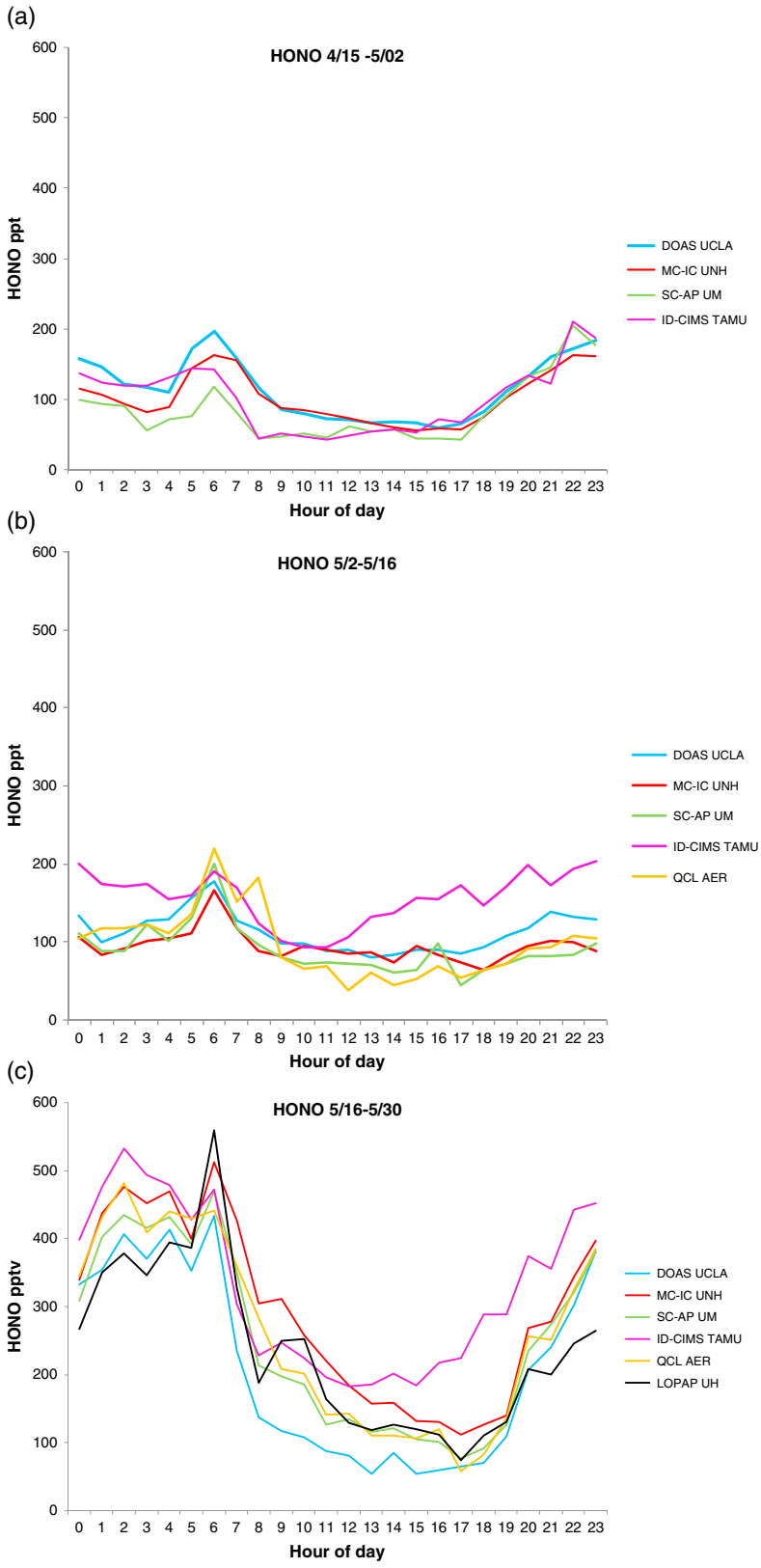


**Figure 2.** (a) Hourly average HONO concentrations measured by instruments operational between 15 April and 2 May. (b) Hourly average HONO concentrations measured by instruments operational between 2 May and 16 May. (c) Hourly average HONO concentrations measured by instruments operational during the CMP.

**Table 2.** Summary Statistics for HONO Concentrations Measured by Different Instruments

| Instrument | Obs | Median | Mean | Std. Dev. | Max | Min | Sampling Period |
|---|---|---|---|---|---|---|---|
| DOAS | 1112 | 130 | 142 | 139 | 1380 | −50 | 4/15–5/30 |
| MC-IC | 1037 | 95 | 157 | 167 | 1382 | 22 | 4/16–5/30 |
| SC-AP | 704 | 94 | 161 | 174 | 1260 | 12 | 4/19–5/30 |
| ID-CIMS | 870 | 142 | 198 | 172 | 1101 | 0.65 | 4/20–5/30 |
| QC-TILDAS | 456 | 124 | 182 | 185 | 1336 | −54 | 5/2–5/30 |
| LOPAP | 273 | 169 | 247 | 238 | 1466 | 3 | 5/16–5/30 |

orthogonal distance regression (ODR) was also used [*Boggs et al.*, 1987]. Regression parameters (slopes and intercepts) for ODR are shown beneath those for OLS regression. As can be seen from Figure 3, there is attenuation of the slope in OLS regression [*Mandel*, 1964] compared to a technique such as ODR that accounts for error in the independent variable. However, a number of conditions could result in sizable over correction when using orthogonal regressions, and regression parameters should not be interpreted only in terms of instrumental error [*Carroll and Ruppert*, 1996]. Note also that the DOAS reported several negative values, occurring mainly from 24 April to 27 April. These negative concentrations were kept in the calculation of summary statistics and regressions shown in the tables to prevent bias. The QC-TILDAS also measured negative concentrations on a few occasions, and these were also kept in the calculation of summary statistics.

Considering all day and night data points during the entire measurement campaign, either form of regression showed varying degrees of agreement between all pairs of instruments for their period of record as can be seen from inspection of Table 3. Higher values for ID-CIMS than for other instruments shown in the

**Table 3.** Regression Relations Between All Pairs of Instruments During Their Entire Period of Operation[a]

| Entire Period | Slope ± SE | Intercept ± SE (ppt) | $R^2$ | $N$ | Period |
|---|---|---|---|---|---|
| MC-DL | 1.0 ± 0.02 | 11 ± 3.9 | 0.72 | 1037 | 4/16–5/30 |
| | 1.2 ± 0.02 | −15 ± 4.1 | | | |
| SC-DL | 0.94 ± 0.02 | 17 ± 4.4 | 0.77 | 704 | 4/19–5/30 |
| | 1.0 ± 0.02 | −0.31 ± 4.4 | | | |
| ID-DL | 0.87 ± 0.03 | 66 ± 5.4 | 0.57 | 870 | 4/20–5/30 |
| | 1.1 ± 0.03 | 25 ± 5.8 | | | |
| QCL-DL | 1.0 ± 0.03 | 1.6 ± 6.9 | 0.73 | 456 | 5/1–5/30 |
| | 1.2 ± 0.03 | −36 ± 7.1 | | | |
| LO-DL | 0.90 ± 0.04 | 38 ± 14 | 0.61 | 273 | 5/17–5/30 |
| | 1.2 ± 0.04 | −23 ± 14 | | | |
| SC-MC | 0.89 ± 0.01 | 0.44 ± 2.4 | 0.94 | 666 | 4/19–5/30 |
| | 0.91 ± 0.01 | −4.4 ± 2.3 | | | |
| ID-MC | 0.84 ± 0.02 | 63 ± 4.2 | 0.73 | 837 | 4/20–5/30 |
| | 0.96 ± 0.02 | 43 ± 4.3 | | | |
| QCL-MC | 0.88 ± 0.02 | 1.6 ± 5.9 | 0.90 | 428 | 5/1–5/30 |
| | 0.93 ± 0.01 | −7.7 ± 4.2 | | | |
| LO-MC | 0.88 ± 0.03 | −25 ± 12 | 0.75 | 260 | 5/16–5/30 |
| | 1.0 ± 0.03 | −71 ± 12 | | | |
| ID-SC | 0.90 ± 0.02 | 78 ± 5.0 | 0.76 | 599 | 4/20–5/30 |
| | 1.0 ± 0.02 | 57 ± 5.2 | | | |
| QCL-SC | 0.98 ± 0.02 | 7.8 ± 5.1 | 0.89 | 349 | 5/1–5/30 |
| | 1.0 ± 0.02 | −4.3 ± 5.2 | | | |
| LO-SC | 0.89 ± 0.04 | 4.5 ± 13 | 0.68 | 261 | 5/16–5/30 |
| | 1.1 ± 0.04 | −56 ± 14.1 | | | |
| QCL-ID | 0.84 ± 0.02 | −35 ± 8.4 | 0.70 | 387 | 5/1–5/30 |
| | 0.97 ± 0.03 | −71 ± 8.9 | | | |
| LO-ID | 0.74 ± 0.05 | −16 ± 23 | 0.45 | 233 | 5/16–5/30 |
| | 1.2 ± 0.07 | −187 ± 28 | | | |
| LO-QCL | 0.87 ± 0.04 | 5.8 ± 16 | 0.66 | 194 | 5/16–5/30 |
| | 1.1 ± 0.05 | −57 ± 18 | | | |

[a]Independent variables are listed in order of their record length, i.e., DOAS, mist chamber, SC-AP, ID-CIMS, QC Laser, and LOPAP (abbreviations: DL, MC, SC, ID, QCL, and LO). All results are highly statistically significant with $P$ values $< 10^{-4}$. Upper entries in split cells refer to OLS regressions and lower entries refer to ODR regressions.

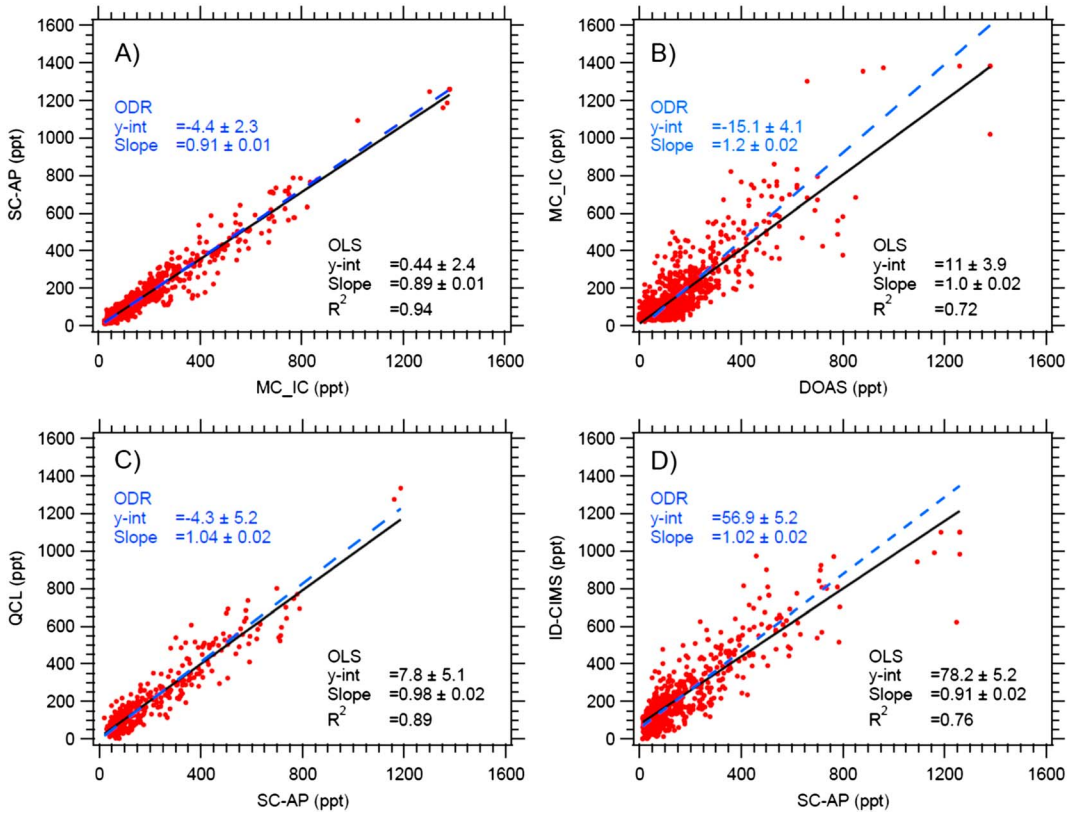


**Figure 3.** Scatterplots showing selected regressions based on data shown in Table 3.

figures are reflected mainly in the large intercepts of its regressions. All results are highly statistically significant with $P$ values $< 10^{-4}$.

Figure 3 shows scatterplots for pairs of in situ measurements showing best agreement with each other, i.e., the mist chamber, SC-AP, and QC-TILDAS, and in comparison of these instruments to DOAS. As can be seen from Table 3, comparisons involving only these three in situ instruments are characterized by higher $R^2$ (~0.9) than for comparisons with the DOAS ($R^2 \sim 0.7$) and coincidentally with much less scatter especially at high concentrations. A number of reasons contribute to this finding, especially differences in the air masses sampled by the in situ instruments and the DOAS. However, plots for all the other instruments are shown in the supporting information (SI). Figures in the SI are ordered according to length of record, i.e., Figure S3 includes data from shortly after inception to the end of the study while Figure S9 includes data taken during the last 2 weeks of the study, i.e., when the LOPAP was operational.

### 3.2. Differences Between Techniques

Figure 4 shows normalized differences (ND) for all times (day + night) between instruments.

$$\mathrm{ND}_{ij} = \left(C_i - C_j\right)/\left(C_i + C_j\right) \tag{1}$$

where $C_i$ refers to HONO concentration measured by one instrument (DOAS, MC-IC, ID-CIMS, SC-AP, LOPAP, and QC-TILDAS) and $C_j$ refers to HONO concentrations measured by another of these instruments. Results only for the instruments shown in Figure 3 are shown in Figure 4, but results for other instruments are shown in the supplementary information (see Figures S10–S13). NDs were also used by *Arnold et al.* [2007] in a field test of methods for measuring nitric acid in the atmosphere. Also shown in Figure 4 are coefficients of divergence (CD), which are a normalized measure of similarity between time series of measurements [*Wongphatarakul et al.*, 1998; *Pinto et al.*, 2004] and are defined as

$$\mathrm{CD}_{ij} = \sqrt{\left((1/p) \times \Sigma \mathrm{ND}_{ij}\right)^2} \tag{2}$$

where $p$ is the number of observations and $\mathrm{ND}_{ij}$ is defined above. A CD of 0 indicates that the two time series

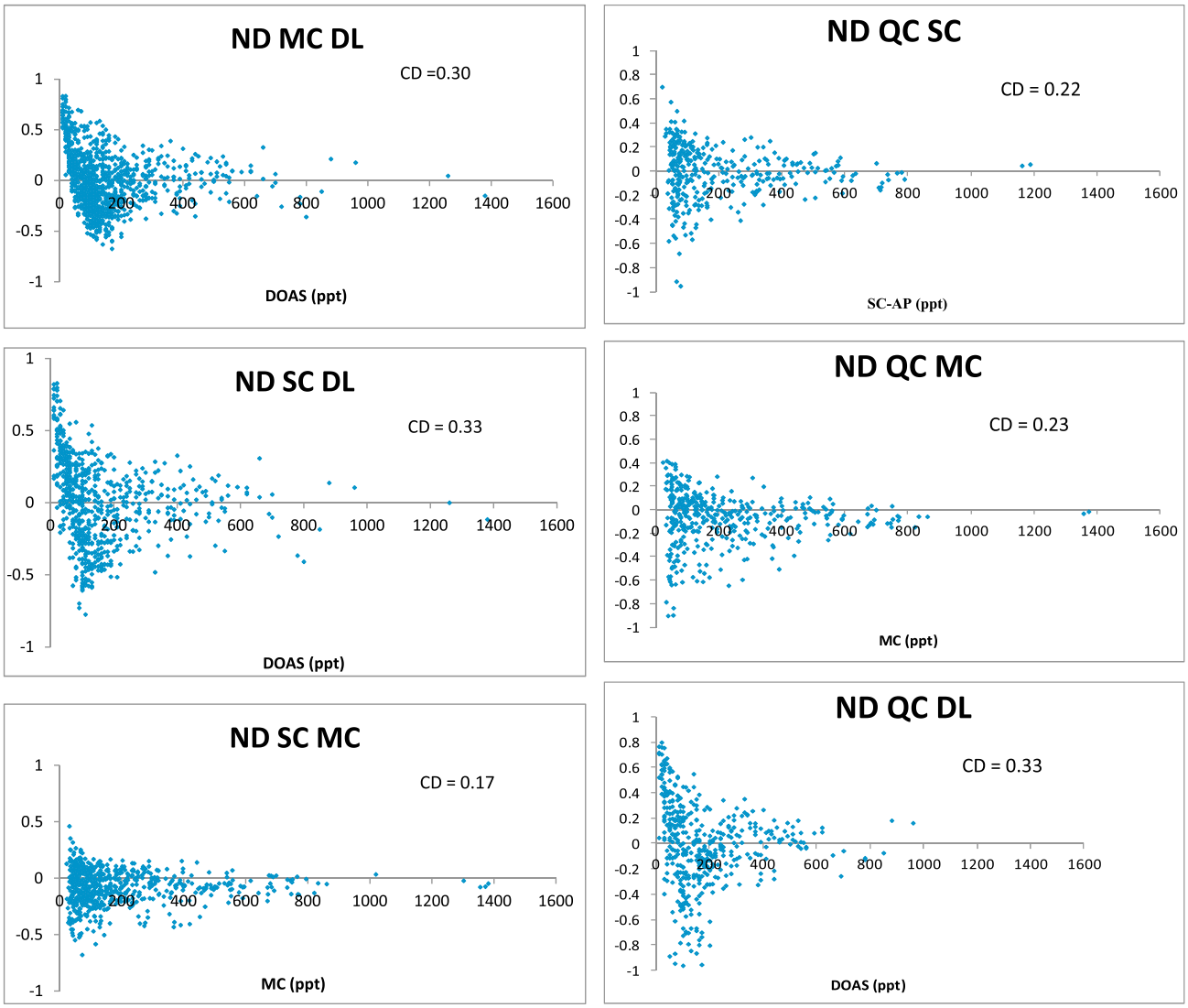


**Figure 4.** Normalized difference between the mist chamber and DOAS, the SC-AP and DOAS, the SC-AP and mist chamber, the QC-TILDAS and SC-AP, the QC-TILDAS and mist chamber, and the QC-TILDAS and DOAS. Also shown is the coefficient of divergence (CD).

are identical, and a CD of 1 indicates they are completely different. This metric tends to place greater weight on lower concentrations in contrast to ordinary least squares regressions. Note the sloping edge in ND at the lowest concentrations for all the instrumental comparisons involving the DOAS with a tendency for the in situ instruments to be higher than the DOAS. This sloping lower edge is not seen for comparisons involving only the in situ instruments. Possible interpretations might be a negative offset in the DOAS measurements by ~ 50 ppt, a positive bias of the in situ instruments (perhaps caused by the placement of sampling inlets near building surfaces) or a general disagreement due to different sampling altitudes and volumes between the DOAS and the in situ systems. Values of CD are lower involving pairs of data from the mist chamber, SC-AP, and QC-TILDAS (0.17–0.23) than for pairs of these instruments involving the DOAS (0.30–0.33) and for pairs of the LOPAP and ID-CIMS with the other in situ instruments (0.27–0.35) and with the DOAS (0.33–0.37). According to this measure, closest agreement was among pairs of the MC-IC, SC-AP, and QC-TILDAS.

### 3.3. Measurements During Daytime in the Common Measurement Period

During the CMP (16 May to 30 May), all instruments were operational. The final 2 weeks of the measurement campaign were arguably the most important for photochemical activity. Mean daytime (0900 to 1700)

**Table 4.** Summary Statistics for 5 to 11 A.M. HONO Concentrations During the Common Measurement Period (16 May to 30 May)[a]

| Instrument | Obs | Median | Mean | Std. Dev. | Max | Min |
|---|---|---|---|---|---|---|
| DOAS | 77 (37) | 160 (270) | 235 (292) | 205 (166) | 1380 (620) | 20 (20) |
| MC-IC | 72 (37) | 362 (397) | 381 (427) | 235 (202) | 1302 (861) | 87 (106) |
| SC-AP | 69 (37) | 276 (351) | 316 (367) | 240 (201) | 1248 (779) | 45 (48) |
| ID-CIMS | 61 (37) | 268 (386) | 335 (392) | 215 (209) | 942 (898) | 56 (56) |
| QC-TILDAS | 56 (37) | 311 (360) | 336 (377) | 183 (187) | 801 (801) | 44 (88) |
| LOPAP | 69 (37) | 240 (289) | 334 (356) | 279 (247) | 1357 (1085) | 22 (22) |

[a]The first set of values shows all data points and the second set in parentheses shows only those when all six instruments were making measurements simultaneously.

temperatures were actually slightly lower than during the preceding 2 weeks (26.5°C versus 28.3°C), winds blew pollutants from the Houston Ship Channel a larger fraction of the time (~44% versus 6%) during the day; photochemistry was more active (mean daytime $O_3$ was higher by ~ 17 ppb and $P(O_3)$ was roughly twice as high) during daytime in the CMP than during weeks 3–4 [*Cazorla et al.,* 2012].

During the CMP, the highest readings by all the instruments occur at night and as noted earlier much clearer differences can be seen between daytime and nighttime measurements than during the first 4 weeks. It might appear initially that the higher nighttime HONO concentrations measured by the DOAS than by the in situ instruments during the first 4 weeks are simply related to more stable stratification in the nocturnal boundary layer especially since HONO is related to primary species whose sources are located mainly at or just above the surface such as motor vehicle exhaust or aerosol surfaces. However, mean nighttime HONO concentrations during the CMP measured by the DOAS are closer to the lower end of the range measured by the in situ instruments indicating either changes in nocturnal stratification or interference in either the DOAS or other techniques from the first 4 weeks. Note though that HONO concentrations measured by different techniques differ by only about 20 to 30%.

Morning, in particular early morning, is the most important time for radical formation from HONO photolysis. As shown in Table 4, median (mean) HONO concentrations measured by all six instruments from 5 to 11 A.M. ranged from 160 (235) ppt for the DOAS to 362 (381) ppt for MC-IC when all available data points were used for each instrument; medians (means) ranged from 270 (292) ppt for DOAS to 397 (420) ppt for MC-IC using only data collected when all six instruments were in operation simultaneously. Medians (means) for the three instruments with collocated inlets (MC-IC, SC-AP, and QC-TILDAS) agreed with the ensemble median (mean) to within 10 to 20% with better agreement when only simultaneously collected data were used. Note the differences in summary statistics when only simultaneous data are used. When data from all six instruments were used, largest differences (ranging from −20% to −40%) with the ensemble mean were obtained for the DOAS. Again, better agreement was obtained when only simultaneously collected data were used. This result could be due to sampling error and to environmental or other external factors adversely affecting

**Table 5.** Regression Relations During the Times Given in Table 4[a]

| Morning CMP | Slope ± SE | Intercept ± SE (ppt) | $R^2$ | $N$ | Slope ± SE | Intercept ± SE (ppt) | $R^2$ |
|---|---|---|---|---|---|---|---|
| MC-IC | 0.92 ± 0.01 | 92 ± 3.6 | 0.81 | 53 | 1.0 ± 0.01 | 51 ± 4.4 | 0.85 |
| | 1.03 ± 0.01 | 55 ± 3.5 | | | 1.1 ± 0.01 | 17 ± 5.1 | |
| SC-AP | 0.95 ± 0.01 | 9.8 ± 3.6 | 0.82 | 50 | 0.97 ± 0.01 | 0.35 ± 5.2 | 0.83 |
| | 1.05 ± 0.01 | −27 ± 3.8 | | | 1.08 ± 0.01 | −39 ± 5.4 | |
| ID-CIMS | 0.88 ± 0.02 | 65 ± 5.5 | 0.68 | 43 | 0.92 ± 0.02 | 46 ± 6.9 | 0.68 |
| | 1.1 ± 0.02 | −7.4 ± 6.4 | | | 1.1 ± 0.02 | −38 ± 8.2 | |
| LOPAP | 0.91 ± 0.02 | 42 ± 7.5 | 0.45 | 53 | 0.98 ± 0.02 | −14 ± 10 | 0.55 |
| | 1.8 ± 0.03 | −180 ± 10 | | | 1.4 ± 0.03 | −189 ± 13 | |
| DOAS | 0.74 ± 0.01 | −1.7 ± 2.7 | 0.73 | 56 | 0.75 ± 0.01 | 9.6 ± 4.4 | 0.72 |
| | 0.85 ± 0.09 | −38 ± 3.3 | | | 0.87 ± 0.01 | 34 ± 8.2 | |

[a]QC-TILDAS is used as the independent variable. Dependent variables shown in far left column. (left) All available pairwise data. (right) Only data collected when all instruments operated simultaneously ($N = 37$). OLS regression parameters shown in upper halves of split cells; ODR parameters shown in lower halves. All results are highly statistically significant with $P$ values $< 10^{-4}$.

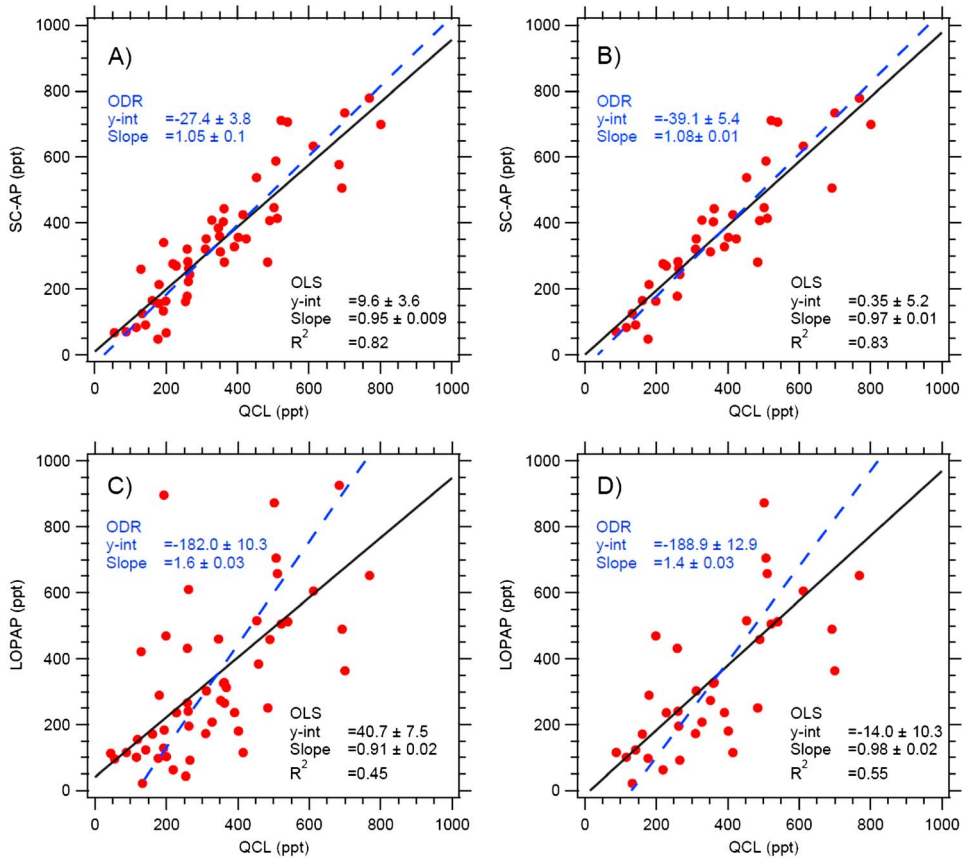


**Figure 5.** Scatterplots showing selected regressions based on data shown in Table 5 for 5 to 11 A.M. during the common measurement period. (a and c) Results for all possible pairs and (b and d) show results when all six instruments were in operation.

performance of individual instruments. Note that the median (mean) HONO concentrations measured by ID-CIMS are within the range of the other instruments. These 5 to 11 A.M. concentrations can be contrasted with those measured during the first 4 weeks of the campaign, in which median (mean) HONO concentrations measured by each instrument ranged from 76 to 110 ppt (93 to 130 ppt) with little dependence on wind direction. Winds were from the east in the general direction of the Houston Ship Channel (wind sector 45° to 135°) 30% of the time from 5 to 11 A.M. during the CMP, compared to only 11% of the time during the preceding 4 weeks of the campaign. Measured HONO concentrations were roughly twice as high when winds were from this sector than from the west during the CMP. In contrast, during the first 4 weeks of the campaign, HONO concentrations showed little dependence on wind direction.

Regression parameters for HONO concentrations measured by the six instruments for 5 to 11 a.m. during the CMP are given for all pairwise comparisons on the left in Table 5 and for those times when all six instruments were in operation simultaneously on the right in Table 5. Scatterplots and sample regressions for these times are shown in Figure 5.

Daytime (0900–1700) median concentrations during the CMP measured by all instruments ranged from 80 ppt (for DOAS-LP) to 177 ppt (for ID-CIMS). As can be seen from Figure 2c, systematically higher values are found by all the in situ instruments than by DOAS; and it is clear that these higher readings occur mainly for lower concentrations measured by DOAS. This is in contrast to the situation in the first 4 weeks of the campaign, during which measurements by DOAS are higher than those measured by the MC-IC, SC-AP, and QC-TILDAS (cf. Figures 2a and 2b). Not only are there differences between the in situ instruments and the DOAS but also differences among themselves—the overwhelming majority of which are statistically significant ($P$ values $< 0.05$) for differences of ~ 20%. HONO concentrations measured by the mist chamber tended to be higher than those measured by SC-AP, and QC-TILDAS, but dependence on wind direction was not consistent. Slightly lower differences for the MC-IC compared to SC-AP were found when winds were

**Table 6a.** Summary of Most Important Factors Based on PCA and Marker Species Explaining Variance in Overall Data Set for Daytime Sampling (0900–1700) During the Common Measurement Period

| Factor Number | | Marker Species |
|---|---|---|
| 1 | Primary | NO, $NO_2$, benzene, toluene, C2-C3 alkylbenzenes, acetaldehyde, HCHO, and HONO |
| 2 | Secondary | $O_3$, $HNO_3$, PAN, $H_2O_2$, and HCHO |
| 3 | Secondary | $CH_3OOH$, and $H_2O_2$ |
| 4 | Primary | Phenol |
| 5 | Primary | Styrene |

from the east than from the west (52 versus 58 ppt), but higher differences (57 ppt versus 20 ppt) compared to QC-TILDAS were found when winds were from the east rather than from the west.

Principal components analysis (PCA) was performed for the period 16 May to 30 May in order to better understand the relationships between HONO and other species during SHARP and perhaps to provide some insight into the nature of possible interfering species. Results are shown in Table 6a for the five factors explaining 75% of the variance in the daytime data set for $NO_z$ species and VOCs. The species identified in the five factors can be conveniently classified as primary or secondary. Factor 1 comprises primary species, possibly from mobile sources—NO, $NO_2$, benzene, toluene, C2-C3 alkylbenzenes, acetaldehyde ($CH_3$-CHO), HCHO, and HONO. Acetaldehyde has long been recognized as a primary component of motor vehicle exhaust, whose emissions have likely increased due to the addition of ethanol to fuel [*de Gouw et al.*, 2012]; formaldehyde has been shown by *Olaguer et al.* [2009, 2013] to be a primary component of combustion emissions sources including internal combustion engines; and *Rappenglück et al.* [2013] identified vehicles as a source of HONO in Houston. *Wong et al.* [2012] found that HONO was derived from ground or other low-lying surface sources. The PCA results described here are also consistent with a ground level or near-surface source for HONO. Factor 2 comprises secondary species—$O_3$, $HNO_3$, PAN, $H_2O_2$, and HCHO. The presence of HCHO in both factors indicates that its sources have both a strong primary component and a strong secondary component, respectively. HONO shows only a weak association with Factor 2. Factor 3 comprises another set of secondary species, namely, peroxides—$CH_3OOH$ and $H_2O_2$. Factor 4 is dominated by phenol and Factor 5 by styrene, both presumably from industrial sources. The composition of these factors suggests that strong collinearity exists among species.

The five main factors explaining the variance in the daytime data set also explain 76% of the variance in the nighttime data set and are shown in Table 6b. Factor 1 is composed of primary species, likely emitted by mobile sources—NO, $NO_2$, benzene, toluene, C2- C3 alkylbenzenes, acetaldehyde, HCHO, and HONO. Factor 2 contains secondary species—$O_3$, $HNO_3$, PAN, and $H_2O_2$. Factor 3 is dominated by $SO_2$, which could be emitted mainly by refineries. Factor 4 is dominated by styrene and $SO_2$ indicating an industrial source for this factor. Factor 5 is dominated by isoprene and monoterpenes. Aerosol composition data that might have helped in the identification of sources were not available.

As noted earlier, the issue of possible interference in chemical techniques has been raised by *Stutz et al.* [2010] and *Kleffmann et al.* [2006]. *Stutz et al.* [2010] related the difference between the MC-IC and the DOAS to individual indicators (e.g., $O_3$ and $HNO_3$) of potential interfering compounds (organic nitrites). Their analysis is repeated here by using forward stepwise regression of differences between in situ instruments and the DOAS (low path) on scores derived from principal components analysis (PCA) of the

**Table 6b.** Summary of Most Important Factors and Marker Species Explaining Variance in Overall Data Set for Nighttime Sampling (2000–0700) During the Common Measurement Period

| Factor Number | | Marker Species |
|---|---|---|
| 1 | Primary | NO, $NO_2$, benzene, toluene, C2-C3 alkylbenzenes, acetaldehyde, HCHO, and HONO |
| 2 | Secondary | $O_3$, $HNO_3$, PAN, and $H_2O_2$ |
| 3 | Primary | $SO_2$ |
| 4 | Primary | Styrene and $SO_2$ |
| 5 | Primary | Isoprene and monoterpenes |

**Table 7.** Regression Analysis of Differences Between In Situ Techniques and the DOAS Based on Factors Given in Table 6a[a]

| Difference | Wind Direction | Factor 1 | Factor 2 | Factor 3 | Factor 4 | Factor 5 | Model $R^2$ |
|---|---|---|---|---|---|---|---|
| | | *Day* | | | | | |
| DOAS-SC-AP | All | 0.24 | 0.36 | 0.05 | 0.08 | 0.02 | 0.76 |
| DOAS-SC-AP | East (Houston Ship Channel (HSC)) | | 0.76 | | | | 0.76 |
| DOAS-SC-AP | Rest | 0.28 | 0.33 | 0.05 | 0.08 | 0.04 | 0.78 |
| DOAS-LOPAP | All | 0.30 | 0.09 | 0.24 | 0.10 | 0.09 | 0.82 |
| DOAS-LOPAP | East (HSC) | | 0.51 | | | 0.27 | 0.78 |
| DOAS-LOPAP | Rest | 0.38 | 0.04 | 0.40 | 0.03 | 0.02 | 0.88 |
| DOAS-MC-IC | All | 0.10 | 0.70 | 0.02 | 0.05 | | 0.86 |
| DOAS-MC-IC | East (HSC) | | 0.90 | | | | 0.90 |
| DOAS-MC-IC | Rest | 0.12 | 0.65 | 0.02 | 0.06 | | 0.85 |

[a] $R^2$ shown for all entries for factors that are statistically significant ($P$ value $< 0.05$).

suite of species listed in section 2.1. Note that all of the in situ instruments show higher mean values than the DOAS for HONO during daytime in the CMP. Table 7 shows partial $R^2$ based on regression of differences between in situ techniques and DOAS on the scores for each of these five components for daytime (0900 to 1700) measurements during the CMP. The photochemical factor (Factor 2) had highest partial $R^2$ for the mist chamber $R^2 = 0.90$, the SC-AP (University of Miami) $R^2 = 0.76$, and LOPAP (University of Houston) $R^2 = 0.51$, when winds were from the east in the sector between 45° and 135°, i.e., when winds were from the Houston Ship Channel. The high $R^2$ for the mist chamber and the LOPAP with the photochemical factor indicate the possibility of chemical interference, though not necessarily that it exists. There were no strong relationships (combined $R^2 > 0.5$) involving these five factors and differences between the ID-CIMS or QC-TILDAS and the DOAS. These results indicate that the much higher concentrations found by ID-CIMS than for other instruments during the day were not related to chemical interference but to other unspecified factors, whereas the QC-TILDAS was not likely subject to appreciable chemical interference. It should be stressed, though, that these results were obtained when daytime HONO concentrations measured by all instruments ranged from $80 \pm 49$ ppt for the DOAS to $206 \pm 92$ ppt for the ID-CIMS, i.e., toward the lower end of the concentration range during the entire campaign. At these low concentrations there is increased likelihood of having compounds that could potentially cause interference, and as noted earlier this does not mean that substantial interference necessarily exists. Also, concentrations can approach stated detection limits for the optical instruments at these low levels (see Table 1).

These results are in accord with *Stutz et al.* [2010] who related the difference between HONO measured during the day by the mist chamber and the DOAS to several trace species individually, most notably to ozone. *Stutz et al.* [2010] attributed differences to the possibility of positive artifact by organic nitrites in the detection of nitrite ions by IC. Thus, if there were a chemical-causing interference resulting in overreporting, its concentration would only need to be about 100 ppt for the mist chamber and about 50 ppt for the SC-AP (assuming an efficiency of one for the interference), if indeed it can be assumed that the differences can be attributed to chemical interference. Organic nitrites, as proposed by *Stutz et al.* [2010], were not sampled and remain candidates for further study. It is not clear what substance would cause the difference between the DOAS and the SC-AP ($R^2 = 0.43$ for $HNO_3$, 0.45 for PAN, and 0.30 for $O_3$). Although the base-catalyzed hydrolysis of PAN yields nitrite [*Roberts*, 1990], posing a possible source of interference for the SC-AP, it used two coil samplers in series and the downstream sampler should remove this interference. Note that the QC-TILDAS also reported mean daytime HONO concentrations higher than DOAS that were similar to those measured by other in situ instruments, but there was no strong association found between the QC-TILDAS-DOAS difference and any other oxidants ($R^2 = 0.086$ for $HNO_3$, 0.076 for PAN, and 0.0001 for $O_3$).

Alternatively, the DOAS could have been subject to negative interference by $NO_2$ as noted by *Kleffmann et al.* [2006]. However, this is unlikely as nighttime HONO measurements made by the DOAS (low path) are very similar to the in situ measurements. $NO_2$ mixing ratios at night are much higher than during the day and thus should worsen this effect, which was not observed. In addition, as shown in *Stutz et al.* [2010, Figure 9] there was essentially no correlation between the difference of the DOAS and the MC systems and $NO_2$ during TexAQS II in 2006. A very similar result was found during SHARP in 2009. In the 2009 results shown here the agreement between the DOAS and the in situ systems is quite good for the first 4 weeks of the experiment.

Since no changes were made to the DOAS system or the analysis procedure for the entire campaign, it is not clear why the DOAS should show interferences only in the last 2 weeks. In addition, we compared days such as 20 May and 21 May, for which $NO_2$ levels were very similar. The daytime DOAS data show little difference in HONO between these 2 days. The in situ data, however, are much higher than the DOAS on 20 May while all the data are quite similar on 21 May. Thus, there is no clear indication that a negative bias in the DOAS data can explain all the differences between DOAS and in situ data. It is also worth reiterating that vertical stratification and heterogeneities across the DOAS light path are other factors that could have contributed to the difference between the DOAS and in situ measurements. Assessing the latter possibility using mechanistic models is beyond the scope of this paper. However, some indication of the likelihood of incomplete vertical mixing can be given by comparisons between primary (surface derived) pollutants, e.g., $NO_2$ and secondary (derived aloft) pollutants, e.g., $O_3$ (cf. Table 6a). Relations between $NO_2$ (measured by QC-TILDAS) and $O_3$ measured in situ on the top of Moody Tower and the DOAS during the daytime of the CMP can be given by

$$O_{3-MT} = 1.12 \pm 0.02 \times \text{DOAS} - 4.10 \pm 1.05 \quad R^2 = 0.97,$$
$$NO_{2-MT} = 0.94 \pm 0.04 \times \text{DOAS} - 0.96 \pm 0.30 \quad R^2 = 0.89.$$

These results suggest that $O_3$ and $NO_2$ locally were relatively well mixed between the altitudes and along the path length sampled by the DOAS and the top of Moody Tower during the day in the CMP. Very similar results for atmospheric mixing are obtained for daytime the preceding 2 week period (see below) when the daytime mean HONO concentration reported by the DOAS was 4.4 ppt higher than the mist chamber, 4.8 ppt higher than the SC-AP and 42 ppt higher than the QC-TILDAS.

$$O_{3-MT} = 1.04 \pm 0.02 \times \text{DOAS} - 0.04 \pm 0.58 \quad R^2 = 0.98,$$
$$NO_{2-MT} = 0.88 \pm 0.20 \times \text{DOAS} - 1.02 \pm 0.09 \quad R^2 = 0.95.$$

Incomplete mixing of HONO as mentioned earlier might also be a possibility that is beyond the scope of this analysis.

## 4. Conclusions

Measurements of HONO made by six instruments during SHARP were compared. Conditions for this study differed from those of the studies of *Kleffmann et al.* [2006] and *Ródenas et al.* [2013] in that this study was conducted entirely under polluted, ambient, and sometimes challenging conditions for 6 weeks. Overall, there was general agreement among all techniques during the measurement campaign. $R^2$ was highest (0.89–0.94) for pairs of MC-IC, SC-AP, and QC-TILDAS and the coefficient of divergence was also lowest (0.17–0.23) for pairs of these instruments, providing another indication of closest agreement among these three instruments. Slopes derived from the two regression techniques (OLS and ODR) were in closest agreement for these three instruments. However, slopes were closest to one for SC-AP and QC-TILDAS (0.98–1.00), but slopes for regressions using MC-IC (as independent variable) were slightly lower (0.88–0.93). Larger deviations are found when the other three instruments, ID-CIMS, LOPAP, and DOAS are considered.

During weeks 3 and 4 of the campaign, the MC-IC, SC-AP, and QC-TILDAS recorded systematically lower values than the DOAS, but during weeks 5 and 6 they recorded higher values, as did the LOPAP, than the DOAS. Means (medians) during the day of the CMP for available measurements of the SC-AP, QC-TILDAS, and LOPAP agreed most closely. Slightly greater deviations in means (medians) were found with respect to MC-IC and even larger deviations for ID-CIMS. Variances in measurements made during the morning of the CMP by the DOAS, MC-IC, SC-AP, ID-CIMS, and QC-TILDAS were comparable while that for the LOPAP was higher. During weeks 3 and 4; HONO concentrations reported by the DOAS, MC-IC, SC-AP, and QC-TILDAS showed little dependence on wind direction. However, during weeks 5 and 6, they reported substantially higher concentrations when winds had an easterly component (a condition that occurred more frequently during the last 2 week period) than when winds were westerly indicating that the Houston Ship Channel could be a source region for HONO.

Large differences in pollution conditions occurred between the first two, 2 week periods and the third, 2 week period. The third period (weeks 5 and 6) in the intercomparison took place under conditions that are unique and challenging, in that the measurement site was subject to high levels of pollutants emitted in the Houston Ship Channel with a larger variety of pollutants than is likely to be found in most locations. These conditions likely

contribute to a greater probability for the presence of compounds causing positive interference in in situ techniques. Alternatively, there could have been negative interference affecting the DOAS, as noted by *Stutz et al.* [2010]. However, there is no clear indication that a negative bias in the DOAS data can explain all the differences between the DOAS and in situ data. The strongest associations with photochemically produced species occur when the winds are easterly, i.e., generally coming off the Houston Ship Channel. Given the similarity in behavior of the Mist Chamber, the QC-TILDAS, the SC-AP, and to a lesser extent, the ID-CIMS and LOPAP with respect to the DOAS, and the difference in their principle of operation, it seems unlikely that it is a question of interference by the same atmospheric species. Likewise, any group of species would have rather tight constraints imposed on the relationships among its members in order to account for the observed differences. Organic nitrites mentioned by *Stutz et al.* [2010] as potential sources of interference in the mist chamber measurements were not measured. Relatively high correlations of some individual species with differences between the SC-AP, the mist chamber and the DOAS, but not with QC-TILDAS, were found. Species correlated with these differences should not necessarily be viewed as causing interference, as they may be surrogates for other species or for a particular set of atmospheric conditions that are also photochemical products. Unless organic nitrites can form HONO during sampling, they are not expected to be a source of interference for the QC-TILDAS as it spectroscopically detects HONO and not nitrite anions (similar in some ways to the DOAS).

Inlets for the MC-IC, SC-AP, and QC-TILDAS were collocated, but inlets for the LOPAP and ID-CIMS were located several meters away on the east side of the roof of Moody Tower and at slightly different elevations. The DOAS was mounted on the opposite side of the building. Building surfaces (including those of the Moody Tower) could be sources of HONO and could have contributed to differences among instruments. Likewise, another experiment could possibly have interfered with the operation of ID-CIMS and possibly with other in situ instruments.

These results indicate that factors other than chemical interference need to be considered in interpreting measurement differences between the point and long-path instruments, or between the point measurements. Although differences between instruments generally tended to be larger than the uncertainties given in Table 1, except perhaps in the upper half of the observed concentration range for instruments whose inlets were collocated, these differences should be viewed in the context of the factors given above. Again, it should be stressed that the results obtained from this study apply strictly only to the particular instruments in use for the specific environmental conditions found in this study and should not be taken to apply to all instruments of a specific type under other sampling conditions.

**Acknowledgments**

We would like to acknowledge the various participants in the SHARP campaign who made data available and Stephen McDow and David Svendsgaard for useful discussions. Funding for SHARP was provided by the State of Texas under the Texas Emissions Reduction Plan (TERP) through the Texas Environmental Research Consortium (TERC). The information in this document has been subjected to review by the National Center for Environmental Assessment, U.S. Environmental Protection Agency, and approved for publication. Approval does not signify that the contents reflect the views of the Agency, nor does mention of trade names or commercial products constitute endorsement or recommendation for use. In addition to data presented in the manuscript and SI, additional information can be obtained from the individual investigators cross referenced in the author list and Table 1. M.O. was supported by an appointment to the Research Participation Program at the Office of Research and Development, U.S. EPA, administered by the Oak Ridge Institute for Science and Education (ORISE) through an interagency agreement between the U.S. DOE and EPA. R.Z. acknowledges additional support from the Robert A. Welch Foundation (A-1417). X.R. acknowledges partial support from the National Science Foundation (AGS-0914619). J.Z. acknowledges support from the National Natural Science Foundation of China (41275142).

## References

Acker, K., et al. (2006), Nitrous acid in the urban area of Rome, *Atmos. Environ.*, *40*(17), 3123–3133.

Alicke, B., U. Platt, and J. Stutz (2002), Impact of nitrous acid photolysis on the total hydroxyl radical budget during the limitation of Oxidant Production/Pianura Padana Produzione di Ozono study in Milan, *J. Geophys. Res.*, *107*(D22), 8196, doi:10.1029/2000JD000075.

Arnold, J. R., B. E. Hartsell, W. T. Luke, S. M. Rahmat Ullah, P. K. Dasgupta, G. L. Huey, and P. Tate (2007), Field test of four methods for gas-phase ambient nitric acid, *Atmos. Environ.*, *41*, 4210–4226.

Aumont, B., F. Chervier, and J. Laval (2003), Contribution of HONO sources to the NOx/HOx/$O_3$ chemistry in the polluted boundary layer, *Atmos. Environ.*, *37*, 487–498.

Boggs, P. T., R. H. Byrd, and R. B. Schnabel (1987), A stable and efficient algorithm for nonlinear orthogonal distance regression, *SIAM J. Sci. Stat. Comput.*, *8*, 152–1078.

Carroll, R. J., and D. Ruppert (1996), The use and misuse of orthogonal regression in linear errors-in-variables models, *Am. Stat.*, *50*, 1–6.

Cazorla, M., W. H. Brune, X.-R. Ren, and B. Lefer (2012), Direct measurement of ozone production rates in Houston in 2009 and comparison with two estimation methods, *Atmos. Chem. Phys.*, *12*, 1203–1212, doi:10.5194/acp-12-1203-2012.

Czader, B. H., B. Rappenglück, P. Percell, D. W. Byun, F. Ngan, and S. Kim (2012), Modeling nitrous acid and its impact on ozone and hydroxyl radical during the Texas Air Quality Study 2006, *Atmos. Chem. Phys.*, *12*, 6939–6951.

de Gouw, J. A., J. B. Gilman, A. Borbon, C. Warneke, W. C. Kuster, P. D. Goldan, and R. A. Harley (2012), Increasing atmospheric burden of ethanol in the United States, *Geophys. Res. Lett.*, *39*, L15803, doi:10.1029/2012GL052109.

Dibb, J. E., R. W. Talbot, and M. H. Bergin (1994), Soluble acidic species in air and snow at Summit, Greenland, *Geophys. Res. Lett.*, *21*, 1627–1630.

Dibb, J. E., E. Scheuer, S. I. Whitlow, M. Vozella, E. Williams, and B. M. Lerner (2004), Ship-based nitric acid measurements in the Gulf of Maine during New England Air Quality Study 2002, *J. Geophys. Res.*, *109*, D20303, doi:10.1029/2004JD004843.

Elshorbany, Y. F., R. Kurtenbach, P. Wiesen, E. Lissi, M. Rubio, G. Villena, E. Gramsch, A. R. Rickard, M. Pilling, and J. Kleffmann (2009), Oxidation capacity of the city air of Santiago, Chile, *Atmos. Chem. Phys.*, *9*, 2257–2273, doi:10.5194/acp-9-2257-2009.

Heland, J., J. Kleffmann, R. Kurtenbach, and P. Wiesen (2001), A new instrument to measure gaseous nitrous acid (HONO) in the atmosphere, *Environ. Sci. Technol.*, *35*, 3207–3212.

Febo, A., C. Perrino, M. Gherardi, and R. Sparapni (1995), Evaluation of a high-purity and high-stability generation system for nitrous acid, *Environ. Sci. Technol.*, *29*, 2390–2395.

Kleffmann, J., J. Heland, R. Kurtenbach, J. C. Lörzer, and P. Wiesen (2002), A new instrument (LOPAP) for the detection of nitrous acid (HONO), *Environ. Sci. Pollut. Res.*, *9*, 48–54.

Kleffmann, J., T. Gavriloaiei, A. Hofzumahaus, F. Holland, R. Koppmann, L. Rupp, E. Schlosser, M. Siese, and A. Wahner (2005), Daytime formation of nitrous acid: A major source of OH radicals in a forest, *Geophys. Res. Lett.*, *32*, L05818, doi:10.1029/2005GL022524.

Kleffmann, J., J. C. Lörzer, P. Wiesen, C. Kern, S. Trick, R. Volkamer, M. Rodenas, and K. Wirtz (2006), Intercomparison of the DOAS and LOPAP techniques for the detection of nitrous acid (HONO), *Atmos. Environ.*, *40*, 3640–3652.

Lee, B. H., E. C. Wood, M. S. Zahniser, J. B. McManus, D. D. Nelson, S. C. Herndon, G. W. Santoni, S. C. Wofsy, and J. W. Munger (2011), Simultaneous measurements of atmospheric HONO and $NO_2$ via absorption spectroscopy using tunable mid-infrared continuous-wave quantum cascade lasers, *Appl. Phys. B*, *102*(2), 417–423.

Lee, B. H., E. C. Wood, M. S. Zahniser, J. Wormhoudt, S. C. Wofsy, and J. W. Munger (2012), Effective line strengths of trans-nitrous acid near 1275 $cm^{-1}$ and cis-nitrous acid at 1660 $cm^{-1}$, *J. Quant. Spectrosc. Radiat. Transfer*, *113*, 1905–1912.

Mandel, J. (1964), *The Statistical Analysis of Experimental Data*, 410 pp., Dover Publications, Mineola, New York.

Mao, J., et al. (2010), Atmospheric oxidation capacity in the summer of Houston 2006: Comparison with summer measurements in other metropolitan studies, *Atmos. Environ.*, *44*, 4107–4115, doi:10.1016/j.atmosenv.2009.01.013.

Molina, M. J., L. T. Molina, R. Zhang, R. Meads, and D. Spencer (1997), Heterogeneous reaction of $ClONO_2$ with HCl on aluminum oxide, *Geophys. Res. Lett.*, *24*, 1619–1622.

Olaguer, E. P., et al. (2009), Deciphering the role of radical precursors during the second Texas Air Quality Study, *J. Air Waste Manage. Assoc.*, *59*, 1258–1277.

Olaguer, E. P., C. E. Kolb, B. Lefer, B. Rappenglück, R.-Y. Zhang, and J. P. Pinto (2013), Overview of the SHARP campaign: Motivation, design, and major outcomes, *J. Geophys. Res. Atmos.*, *119*, 2597–2610, doi:10.1002/2013JD019730.

Pinto, J. P., A. S. Lefohn, and D. Shadwick (2004), Spatial variability of $PM_{2.5}$ in U.S. urban areas, *J. Air Waste Manage. Assoc.*, *54*, 440–449.

Platt, U., and J. Stutz (2008), *Differential Optical Absorption Spectroscopy: Principles and Applications*, Springer, Heidelberg, N. Y.

Platt, U., D. Perner, G. W. Harris, A. M. Winer, and J. N. Pitts Jr. (1980), Observations of nitrous acid in an urban atmosphere by differential optical absorption, *Nature*, *285*, 312–314.

Rappenglück, B., G. Lubertino, S. Alvarez, J. Golovko, B. Czader, and L. Ackermann (2013), Radical precursors and related species from traffic as observed and modeled at an urban highway junction, *J. Air Waste Manage. Assoc.*, *63*, 1270–1286, doi:10.1080/10962247.2013.822438.

Ren, X., et al. (2010), Measurement of nitrous acid at Blodgett Forest during BEARPEX2007, *Atmos. Chem. Phys.*, *10*, 6283–6294.

Ren, X., et al. (2013), Atmospheric oxidation chemistry and ozone production: Results from SHARP 2009 in Houston, Texas, *J. Geophys. Res. Atmos.*, *118*, 5770–5780, doi:10.1002/jgrd.50342.

Roberts, J. M. (1990), The atmospheric chemistry of organic nitrates, *Atmos. Environ.*, *24A*, 243–287.

Ródenas, M., A. Munoz, F. Alacreu, T. Brauers, H.-P. Dorn, J. Kleffmann, and W. Bloss (2013), Assessment of HONO measurements: The FIONA campaign at EUPHORE, in *Disposal of Dangerous Chemicals in Urban Areas and Mega Cities*, NATO Science for Peace and Security Series C: Environmental Security, edited by I. Barnes and K. J. Rudzinski, pp. 45–58, Springer Science and Business Media, Dordrecht, The Netherlands, doi:10.1007/978-94-007-5034-0_4.

Scheuer, E., R. W. Talbot, J. E. Dibb, G. K. Seid, L. DeBell, and B. Lefer (2003), Seasonal distributions of fine aerosol sulfate in the North American Arctic basin during TOPSE, *J. Geophys. Res.*, *108*(D4), 8370, doi:10.1029/2001JD001364.

Stutz, J., H.-J. Oh, S. I. Whitlow, C. Anderson, J. E. Dibb, J. H. Flynn, B. Rappenglück, and B. Lefer (2010), Simultaneous DOAS and mist-chamber IC measurements of HONO in Houston, TX, *Atmos. Environ.*, *44*, 4090–4098.

Wang, L., V. Lal, A. F. Khalizov, and R. Zhang (2010), Heterogeneous chemistry of alkylamines with sulfuric acid: Implications for atmospheric formation of alkylaminium sulfates, *Environ. Sci. Technol.*, *44*, 2461–2465, doi:10.1021/es9036868.

Wong, K. W., C. Tsai, B. Lefer, C. Haman, N. Grossberg, W. H. Brune, X. Ren, W. Luke, and J. Stutz (2012), Daytime HONO vertical gradients during SHARP 2009 in Houston, TX, *Atmos. Chem. Phys.*, *12*, 635–652.

Wongphatarakul, V., S. K. Friedlander, and J. P. Pinto (1998), A comparative study of PM2.5 Ambient aerosol chemical databases, *Environ. Sci. Technol.*, *32*, 3926–3934.

Zhang, R., M. T. Leu, and L. F. Keyser (1996), Heterogeneous chemistry of HONO on liquid sulfuric acid: A new mechanism of chlorine activation on stratospheric sulfate aerosols, *J. Phys. Chem.*, *100*, 339–345.

Zhao, J., and R. Zhang (2004), Proton transfer reaction rate constants between hydronium ion ($H_3O^+$) and volatile organic compounds (VOCs), *Atmos. Environ.*, *38*, 2177–2185.

Zhao, J., N. P. Levitt, and R. Zhang (2005), Heterogeneous chemistry of octanal and 2, 4-hexadienal with sulfuric acid, *Geophys. Res. Lett.*, *32*, L09802, doi:10.1029/2004GL022200.

Zheng, J., et al. (2008), Measurements of $HNO_3$ and $N_2O_5$ using ion drift-chemical ionization mass spectrometry during the MCMA-2006 campaign, *Atmos. Chem. Phys.*, *8*, 6823–6838.

Zhou, X. L. (2013), An overview of techniques for measuring atmospheric nitrous acid, in *Disposal of Dangerous Chemicals in Urban Areas and Mega Cities*, NATO Science for Peace and Security Series C: Environmental Security, edited by I. Barnes and K. J. Rudziński, pp. 29–44, Springer Science and Business Media, Dordrecht, The Netherlands, doi:10.1007/978-94-007-5034-0_3.

Zhou, X. L., Y. He, C. Huang, T. D. Thornberry, M. A. Carroll, and S. B. Bertman (2002), Photochemical production of HONO on glass sample manifold walls, *Geophys. Res. Lett.*, *29*(14), 1681, doi:10.1029/2002GL015080.